JPNT 8(2), 79-85 (2019)
https://doi.org/10.11003/JPNT.2019.8.2.79

JPNT Journal of Positioning, Navigation, and Timing

Multi-constellation Local-area Differential GNSS for Unmanned Explorations in the Polar Regions

Dongwoo Kim, Minchan Kim, Jinsil Lee, Jiyun Lee†

Department of Aerospace Engineering, KAIST, Daejeon 34141, Korea

ABSTRACT

The mission tasks of polar exploration utilizing unmanned systems such as glacier monitoring, ecosystem research, and inland exploration have been expanded. To facilitate unmanned exploration mission tasks, precise and robust navigation systems are required. However, limitations on the utilization of satellite navigation system are present due to satellite orbital characteristics at the polar region located in a high latitude. The orbital inclination of global positioning system (GPS), which was developed to be utilized in mid-latitude sites, was designed at 55°. This means that as the user is located in higher latitudes, the satellite visibility and vertical precision become worse. In addition, the use of satellite-based wide-area augmentation system (SBAS) is also limited in higher latitude regions than the maximum latitude of signal reception by stationary satellites, which is 70°. This study proposes a local-area augmentation system that additionally utilizes Global Navigation Satellite System (GLONASS) considering satellite navigation system environment in Polar Regions. The orbital inclination of GLONASS is 64.8°, which is suitable in order to ensure satellite visibility in high-latitude regions. In contrast, GLONASS has different system operation elements such as configuration elements of navigation message and update cycle and has a statistically different signal error level around 4 m, which is larger than that of GPS. Thus, such system characteristics must be taken into consideration to ensure data integrity and monitor GLONASS signal fault. This study took GLONASS system characteristics and performance into consideration to improve previously developed fault detection algorithm in the local-area augmentation system based on GPS. In addition, real GNSS observation data were acquired from the receivers installed at the Antarctic King Sejong Station to analyze positioning accuracy and calculate test statistics of the fault monitors. Finally, this study analyzed the satellite visibility of GPS/GLONASS-based local-area augmentation system in Polar Regions and conducted performance evaluations through simulations.

Keywords: GPS, GLONASS, polar regions, integrity, local-area differential GNSS

1. INTRODUCTION

The mission tasks of polar exploration and research utilizing unmanned systems have been expanded due to the advantages of unmanned system that can replace human tasks in regions where humans are difficult to access. The missions that utilize an unmanned system include sea ice monitoring and geological exploration using drone aerial shots (Lei et al. 2011, Lucieer et al. 2014). To utilize an unmanned system, a precise and robust navigation system is required. However, the use of satellite navigation systems is limited due to the satellite orbital characteristics at Polar Regions located in high latitudes. For GPS whose designed orbital inclination is 55°, satellite visibility and vertical precision are degraded further as users are located in high latitudes (Reid et al. 2015). The satellite-based augmentation system (SBAS) is also difficult to be used in high-latitude regions as the stationary satellite signal reception quality is

Received Feb 26, 2019 **Revised** Mar 06, 2019 **Accepted** Mar 08, 2019
†**Corresponding Author**
E-mail: jiyunlee@kaist.ac.kr
Tel: +82-42-350-3725 Fax: +82-42-350-3710
Dongwoo Kim https://orcid.org/0000-0002-3257-8195
Minchan Kim https://orcid.org/0000-0001-6447-0966
Jinsil Lee https://orcid.org/0000-0001-6313-4813
Jiyun Lee https://orcid.org/0000-0002-2291-3623

limited (Sundlisæter et al. 2012).

To overcome the limited satellite navigation environment in Polar Regions, a study was conducted to improve positioning accuracy by utilizing multi-constellations such as GLONASS, Galileo, and Beidou in addition to global positioning system (GPS) (Gao et al. 2012). In particular, the orbital inclination of GLONASS is 64.8°, which is suitable in order to ensure satellite visibility in high-latitude regions. A previous study on polar navigation focused on improvements of accuracy in navigation systems. However, accuracy as well as data integrity to cope with navigation fault should also be ensured for the safety of missions by utilizing unmanned systems. Thus, this study designed a multi-constellation local area differential global navigation satellite system (GNSS) utilizing GLONASS additionally.

This study also analyzed the visibility of GPS/GLONASS in Polar Regions through simulations. In addition, re-calculation of fault monitoring statistics and methodology to improve algorithm that should be considered additionally in the local-area differential GNSS when using GLONASS in Polar Regions were presented. Following this, accuracy of the navigation in the local-area differential GNSS system based on GNSS observation data recorded in the Antarctic King Sejong Station was analyzed considering the actual system operation, and performance evaluation on simulation-based availability was conducted.

2. ANALYSIS ON SATELLITE VISIBILITY IN POLAR REGIONS

The satellite visibility, which affects the performance of GNSS the most, differs between mid-latitude and Polar Regions. In particular, the visibility of GPS, which was focused on the utilization in the mid-latitude regions, has been known to be significantly degraded in Polar Regions. Accordingly, the visibility of GPS and GLONASS satellites constellations was analyzed through simulations based on the location of the King Sejong Station regular observatory to analyze the satellite visibility in Polar Regions. Table 1 presents the precise location of the King Sejong Station's regular observatory. In the simulation, almanacs of 24 GPS satellites and 23 GLONASS satellites according to the Radio Technical Commission for Aeronautics (RTCA) standards were used, and the receiver elevation angle was set to 5°.

Fig. 1 shows the daily change trend of vertical dilution of precision (DOP), in which the color of each line refers to the combination of satellite constellations used in DOP calculation. The value of DOP was raised rapidly up to three at certain time period when GPS or GLONASS is utilized

Table 1. Surveyed location of Sejong station.

Latitude (DMS)	Longitude (DMS)	Altitude (m)
62° 13′ 62.2920″ S	58° 47′ 30.1490″ W	26.6626

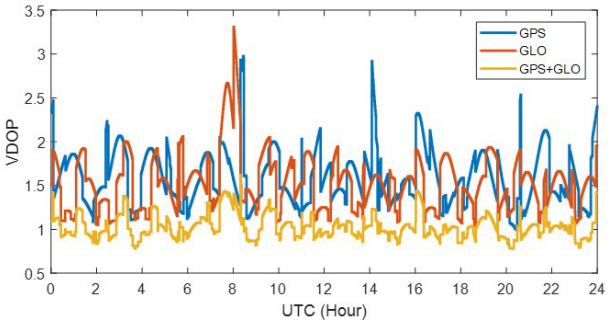

Fig. 1. Vertical dilution of precision (VDOP) at Sejong station.

alone, whereas it was below 1.5 at all time when the two satellite constellations were used. No significant difference was revealed between GLONASS and GPS constellations in the high latitude region because the latitude of the King Sejong Station, which was set to the reference location where the simulation was performed, was 62°, which was not a polar high-latitude region. Thus, the above result implies that if mission tasks are performed at higher latitudes, the satellite visibility will improve further by using GPS and GLONASS together instead of using a single GPS.

3. MULTI–CONSTELLATION LOCAL–AREA DIFFERENTIAL GNSS

3.1 Calculation of Pseudo-range Correction

The local-area differential GNSS generates code correction information of errors every 0.5 sec from ground stations that know the precise locations in advance and broadcasts the code augmentation information to nearby GNSS users. The correction information includes ionospheric delay, tropospheric delay, satellite clock and position error, which are large error elements whose spatial correlation is large, and they are calculated through the following methods.

The code-carrier smoothing filter procedure is conducted beforehand to reduce the noise level of pseudo range measurement in the code correction information calculation. The k-th clock's filtered code measurement ($\tilde{\rho}$) is calculated by a weight sum of the current epoch's code measurement and carrier change-added filtered code measurements at the previous epoch as presented in Eq. (1).

$$\tilde{\rho}(k) = \frac{1}{n}\rho(k) + \frac{n-1}{n}\{\lambda\phi(k) - \lambda\phi(k-1) + \tilde{\rho}(k-1)\} \quad (1)$$

where n refers to the filter's time constant, and λ refers to the signal wavelength. The code correction information (ρ_{corr}) is defined as presented in Eq. (2).

$$\rho_{corr} = \tilde{\rho} - r - c\delta t_{sv} \tag{2}$$

where $\tilde{\rho}$ Refers to the filtered code, r refers to the distance between ground station and satellite, c refers to the light velocity, and δt_{sv} refers to the satellite clock error estimate. The distance between ground station and satellite (r) is directly calculated by a distance from the precise location (x_{ref}) of the ground station to the satellite position (x_{sv}) calculated through the navigation message at the corresponding time.

$$r = \left\| x_{ref} - x_{sv} \right\| \tag{3}$$

The satellite clock error is calculated using the clock error estimate constant included in the navigation message. For GPS, the satellite clock error is calculated using the coefficients of the second order polynomial including the error term (δt_{rel}) due to the relativity principle, whereas the satellite clock error is estimated uisng the coefficients of the first order polynomial only.

$$\begin{aligned} \delta t_{sv,GPS} &= a_0 + a_1 t_k + a_2 t_k^2 + \delta t_{rel} \\ \delta t_{sv,GLO} &= -\tau_n + \gamma_n t_k \end{aligned} \tag{4}$$

3.2 Fault-monitoring Algorithm

The fault monitoring algorithm in local-area differential GNSS largely consists of signal quality monitor (SQM), data quality monitor (DQM), and measurement quality monitor (MQM). In MQM, code-carrier divergence (CCD) monitor, carrier-smoothed code (CSC) innovation test, and carrier acceleration-step test are included (Pullen et al. 2013). This study briefly describes the algorithm for the calculation of test statistic in MQM where additional considerations are generated as GLONASS constellation is added.

The CCD monitor is a monitor that detects the CCD anomaly caused by the satellite clock drift or severe environmental change in the ionosphere. The test statistic (Z_i) of CCD monitor in the i-th satellite at time k is calculated using Eq. (5).

$$\begin{aligned} Z_i(k) = &\left(1 - \frac{1}{\tau_{ccd}} Z_i(k-1)\right) \\ &+ \frac{1}{\tau_{ccd}} \left(\left(\rho_i(k) - \lambda\phi_i(k)\right) - \left(\rho_i(k-1) - \lambda\phi_i(k-1)\right) \right) \end{aligned} \tag{5}$$

where τ_{ccd} refers to the time constant of CCD monitor. The CSC innovation test is a test that detects a sudden change in filtered code measurements. The test statistic (δ_i) of CSC innovation test with regard to the i-th satellite at epoch t is calculated by Eq. (6).

$$\delta_i(t) = \rho_i(t) - (\tilde{\rho}_i(t-1) + \phi_i(t) - \phi_i(t-1)) \tag{6}$$

The carrier acceleration-step test detects a sudden change in impulse, step, and excessive acceleration in the carrier measurement by observing the pattern of changes in continuous carrier correction information value. Such abnormal measurements may act as an error factor of code correction information. The carrier correction information ($\phi_{corr,i}$) with regard to the i-th satellite at epoch t is calculated through Eq. (7).

$$\begin{aligned} \lambda\phi_{ca,i}(t) &= \lambda\phi_i(t) - r_i(t) - c\delta t_{sv,i}(t) - \lambda\phi_{ca,i}(0) \\ \lambda\phi_{corr,i}(t) &= \lambda\phi(t) - \frac{1}{N_{S_j}} \sum_{i \in S_j} \phi_{ca,i}(t) \end{aligned} \tag{7}$$

where S_j refers to the set of the same satellite constellation and N_{S_j} refers to the number of visible satellites in the corresponding constellation at current time.

Three types of test statistics are obtained by fitting the 10 continuous carrier correction information values to the second-order polynomial as presented in Eq. (6). The coefficient in Eq. (8) is solved by the least square method.

$$\phi_{corr,i} = \phi_{corr,i,0} + \frac{d\phi_{corr,i}}{dt} t + \frac{d^2\phi_{corr,i}}{dt^2} \frac{t^2}{2} \tag{8}$$

The three types of test statistics in the carrier acceleration-step test are defined as presented in Eq. (9).

$$\begin{aligned} \mathrm{Acc}_i &\equiv \frac{d^2\phi_{corr,i}}{dt^2} \\ \mathrm{Ramp}_i &\equiv \frac{d\phi_{corr,i}}{dt} \\ \mathrm{Step}_i &\equiv \phi_{corr,i} - \phi_{predicted\_corr,i} \end{aligned} \tag{9}$$

4. ANALYSIS ON NAVIGATION ACCURACY AND PERFORMANCE EVALUATION ON THE SYSTEM

4.1 Data

The GNSS observation data recorded at the Antarctic King Sejong Station were used to verify the accuracy of multi-constellation-based local-area differential GNSS system and calculate the statistics of fault monitoring. The GNSS receiver that corresponded to the user and the ground station was installed at fixed point, and measurements of GPS and GLONASS L1/L2 signals for about four days in January 2018

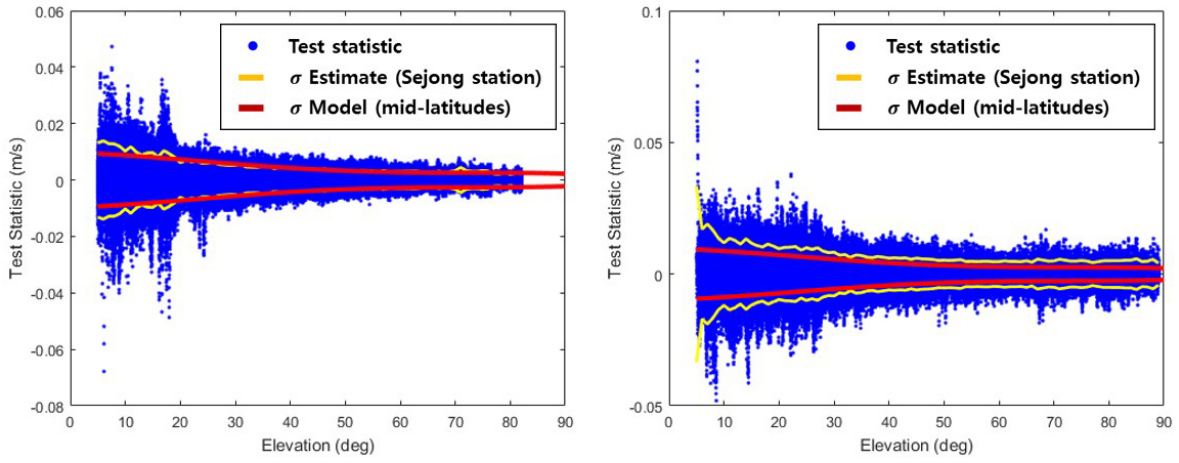

Fig. 2. Test statistics of CCD monitor for GPS (left) and GLONASS (right).

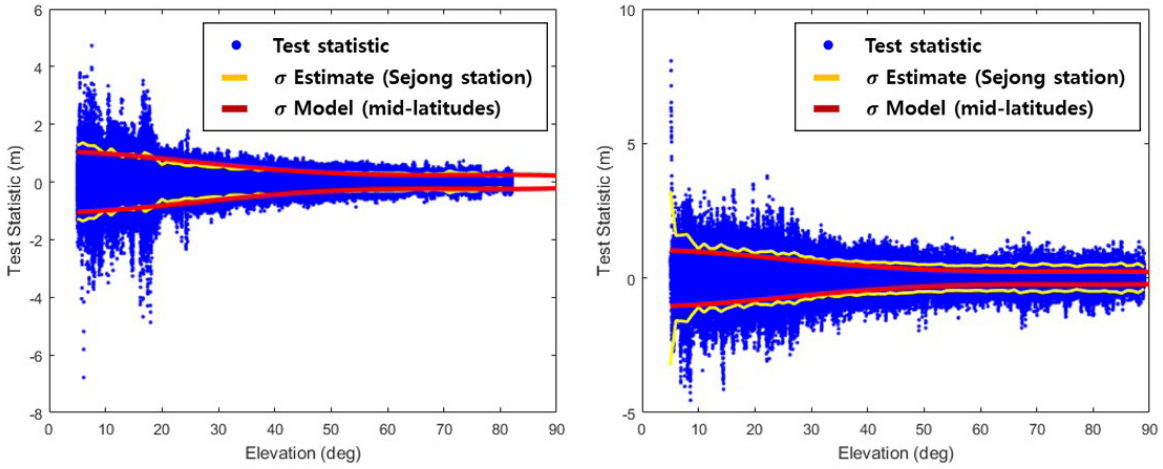

Fig. 3. Test statistics of carrier-smoothed code innovation monitor for GPS (left) and GLONASS (right).

were recorded as the Receiver Independent Exchange Format (RINEX). The receiver model was TOPCON Hiper V, and the observation data were recorded at 1-second intervals. The precise locations of the ground station and user receiver were used to create code correction information and calculate an error of navigation solution, respectively.

4.2 Test Statistics of Fault-monitoring Algorithm

Since the test statistics of the fault monitoring algorithm is a variable that reflects the environment of corresponding region, a process to calculate appropriate statistics should be included in regions where the actual system is operated. Thus, test statistics in CCD monitor and CSC innovation test were calculated using GNSS observation data recorded in the King Sejong Station, and standard deviation calculation results were described accordingly.

Figs. 2 and 3 show the test statistics in CCD monitor and CSC innovation test calculated using actual GNSS data recorded in the King Sejong Station regular observatory in the form of distribution according to the satellite elevation angle. The yellow line marks the statistics calculated through the data, and the red line displays the existing statistic model used in mid-latitude regions. The GPS in the left side verified that the actual measured data statistics were closer to the existing statistics except for some low elevation angle sections whose noise were large. In contrast, GLONASS showed that the actual measured data statistics were larger than existing values at all elevation angle sections. This was due to the larger signal-in-space error of GLONASS than that of the GPS (Kim et al. 2015), which implied that the statistics that reflect the performance of GLONASS system should be applied to GLONASS monitor.

Although the results verified that no significant differences were revealed compared to those of existing models even considering the fact that there were obstacles around the

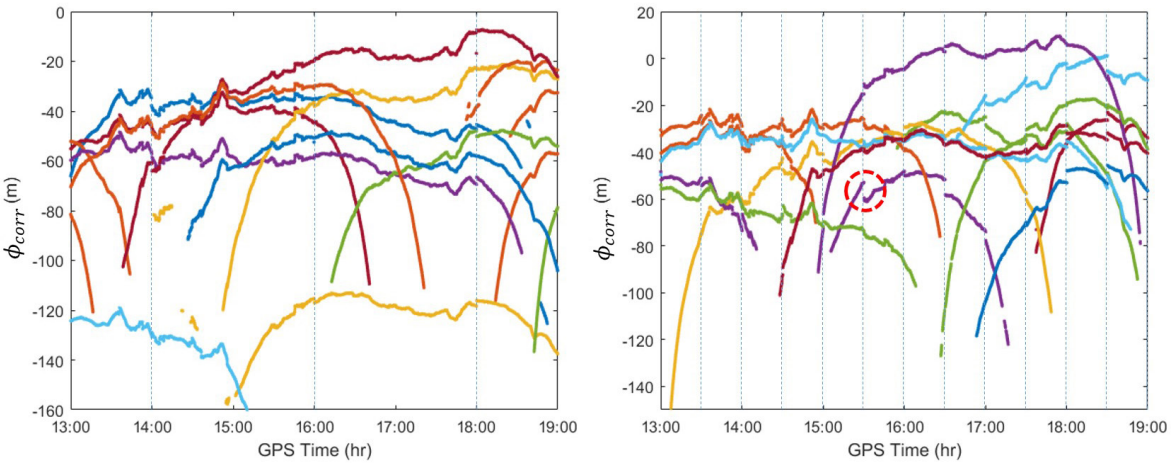

Fig. 4. Trend of ϕ_{corr} for each satellite of GPS (left) and GLONASS (right). Dashed circle indicates an example of the unexpected inconsistency between adjacent GLONASS broadcast ephemeris.

receiver in the installed ground station, it is necessary to reflect data processing results for a longer period in a ground station installation environment without obstacles to acquire statistics that can be used in actual operation.

4.3 Modification of Carrier Acceleration-step Test

If the algorithm designed to detect a fault in existing GPS measurements is applied to GLONASS measurements without modification, it may cause a problem due to the difference in characteristics and performance between GPS and GLONASS systems. For example, existing algorithms in the carrier acceleration-step test is applied to GLONASS measurement, false alarms may occur at specific circumstances due to the difference in characteristics and performance of GLONASS system. Fig. 4 shows the trend of change in the carrier correction per satellite calculated utilizing one-sec GNSS data at Daejeon regular observatory, in which the blue colored dotted line refers to the time when the satellite ephemeris is updated. As mentioned above, the carrier monitor performs polynomial fitting using the continuous carrier correction information value, and a rapid change in the carrier correction information is detected using the test statistics based on the calculated polynomial fitting coefficient. However, discontinuous times occurred as marked in the red circle due to the inaccurate satellite position and clock error estimation during the satellite ephemeris update as shown in the right side figure in Fig. 4. When polynomial fitting is performed in a section where the discontinuous points are included, a large fitting coefficient is calculated. As a result, the test statistics exceed the monitor's threshold even in a situation where the drift of actual satellite clock does not occur.

To prevent such monitor malfunction, the proposed GLONASS carrier monitor's improvement strategy is presented in Table 2. Since a jump occurs at the time when GLONASS satellite ephemeris is updated, a section that includes the corresponding times is determined. Subsequently, the carrier correction information is calculated by re-generating the continuous 10 satellite positions and clock errors by employing the updated ephemeris for the corresponding section. The monitor malfunction is prevented by reflecting the same ephemeris to the test statistics.

Table 2. Strategy for preventing false alarm due to GLONASS ephemeris update.

Order	Content
1	Check the current time whether it is in the effect of the ephemeris update time that possibly causes discontinuity on the carrier-corrections.
2	Produce the satellite orbit and clock correction for the last 10 continuous epochs using the updated ephemeris to obtain the continuous carrier-corrections.
3	Use newly-generated 10 continuous carrier-corrections to fit the quadratic model.

5. PERFORMANCE ASSESSMENT

5.1 Positioning Accuracy

The navigation solution error was calculated with two methods: stand-alone and differential positioning for GPS only use and combined GPS/GLONASS use to verify the navigation solution accuracy. Table 3 presents the 2σ of the errors of the calculated navigation solution for about four days in horizontal and vertical directions. In the stand-alone positioning, which did not use the differential code correction information, the errors of horizontal and vertical accuracies were around 0.7 m and 2.3 m, respectively. When

Table 3. 95% accuracy for the three different positioning methods.

95% Accuracy (2-sigma)	Stand-alone (GPS only)	DGNSS (GPS only)	DGNSS (GPS+GLO)
Horizontal error (m)	0.71	0.27	0.20
Vertical error (m)	2.30	0.95	0.88

Table 4. Vertical protection level (VPL) simulation configuration.

Ground model	Distance	User velocity	PHMI	Constellation	User location
GAD-A	1 km	15 m/s		RTCA 24+23	Sejong station

the differential code correction information was applied, the horizontal and vertical accuracies were 0.3 m and 1 m, respectively, which verified the errors were reduced. In addition, when GLONASS was utilized additionally, the horizontal and vertical accuracies were 0.2 m and 0.9 m, respectively, which verified further reduction. The gains according to the additional use of GLONASS at the latitude region (62° south latitude) where the King Sejong Station was located were not that significant. However, the gains are expected to increase at higher latitude regions where GPS reception range is further limited.

5.2 Positioning Uncertainty

The simulation of vertical protection level (VPL) calculation for one day at the location of the Antarctic King Sejong Station was conducted to evaluate a level of uncertainty of navigation solution. Table 4 presents the simulation conditions set up considering the actual operation circumstances of unmanned system in Polar Regions. The GLONASS error model was set to a 1.5 times larger value than that of the GPS error model considering the performance difference in system accuracy (ESA Navipedia 2011). Fig. 5 shows the daily VPL change trend that can be secured according to the combination of satellite constellations by users located around 1 km away from the ground station. When a single satellite constellation was used, there were times that the VPL was raised suddenly. However, when two satellite constellations were used together, there were gains of 1.4 m in minimum and 8.5 m in maximum while maintaining the VPL around 6 m.

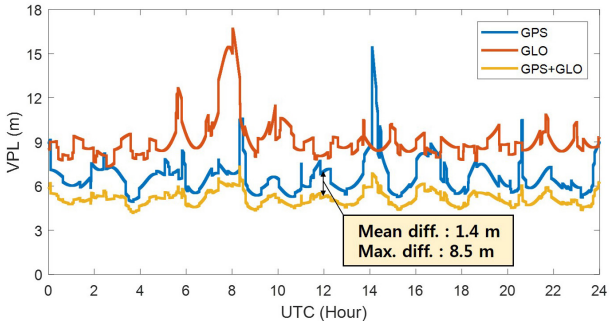

Fig. 5. Vertical protection level (VPL) at Sejong station. The benefit from using GLONASS constellation is 1.4 m in average and 8.5 m of maximum.

6. CONCLUSION

This study proposed a multi-constellation local-area differential GNSS by utilizing GPS and GLONASS to support unmanned exploration in polar regions. First, this study verified that uniform satellite visibility could be obtained for all time periods if GPS and GLONASS were used in Polar Regions through the simulations of satellite visibility analysis in the Antarctic King Sejong Station. Second, the methodology that calculated code correction information and the algorithm that ensured data integrity in the local-air augmentation system were described, and new considerations due to the difference in characteristics and performance between systems when utilizing GLONASS were discussed. The first consideration was that GLONASS monitoring statistics was calculated based on GNSS data observed at the King Sejong Station, and verified that GLONASS monitoring statistics should be larger than the existing GPS statistics in mid-latitude regions. The next consideration was that if the carrier acceleration-step test algorithm was applied to GLONASS without modification, false alarm may occur when the satellite ephemeris was modified. To prevent this, this study proposed an improved methodology by utilizing the same satellite ephemeris. Finally, this study verified the applicability of GPS/GLONASS local-area differential GNSS at Polar Regions through the evaluation on the actual measured data-based navigation accuracy, and the simulation-based navigation solution uncertainty level.

ACKNOWLEDGMENTS

This work was supported by the Korea Polar Research Institute (KOPRI, PE19900).

AUTHOR CONTRIBUTIONS

Dongwoo Kim contributed to the conceptualization of the idea, implemented the software and wrote the original draft of the manuscript. Minchan Kim and Jinsil Lee contributed to the development of the system algorithm and assisted writing the original draft preparation. Jiyun Lee supervised

the research and reviewed the manuscript as a project administrator. All authors discussed the proposed approach and results.

CONFLICTS OF INTEREST

The authors declare no conflict of interest.

REFERENCES

European Space Agency (ESA) Navipedia, GLONASS Performance [Internet], 2011, available from: https://gssc.esa.int/navipedia/index.php/GLONASS_Performance#cite_note-SDCM-3

Gao, G., Heng, L., Walter, T., & Enge, P. 2012, Breaking the Ice: Navigation in the Arctic, Global Navigation Satellite Systems: Report of a Joint Workshop of the National Academy of Engineering and the Chinese Academy of Engineering (Washington D.C., United States: National Academies Press)

Kim, D., Lee, K., Jang, J., & Lee, J. 2015, Characterization of GLONASS Clock and Ephemeris Error for Advanced Receiver Autonomous Integrity Monitor (ARAIM), ISGNSS 2015, Kyoto, Japan.

Lei, X., Bai, L., Du, Y., Miao, C., Chen, Y., et al. 2011, A Small Unmanned Polar Research Aerial Vehicle based on the Composite Control Method, Mechatronics, 21, 821-830. https://doi.org/10.1016/j.mechatronics.2010.12.002

Lucieer, A., Turner, D., King, D., & Robinson, S. 2014, Using an Unmanned Aerial Vehicle (UAV) to capture micro-topography of Antarctic moss beds, International Journal of Applied Earth Observation and Geoinformation, 27, 53-62. https://doi.org/10.1016/j.jag.2013.05.011

Pullen, S., Enge, P., & Lee, J. 2013, High-Integrity Local-Area Differential GNSS Architectures Optimized to Support Unmmaned Aerial Vehicles (UAVs), ION ITM 2013, San Diego, CA.

Reid, T., Walter, T., Blanch, J., & Enge, P. 2016, GNSS Integrity in The Arctic, Navigation, 63, 469-492 https://doi.org/10.1002/navi.169

Sundlisæter, T., Reid, T., Johnson, C., & Wan, S. 2012, GNSS and SBAS System of Systems: Considerations for Applications in the Arctic, Available at SSRN 2228890, 63rd International Astronautical Congress, Oct. 3 2012, At Naples, Italy. https://doi.org/10.2139/ssrn.2228890

Dongwoo Kim received the B.S. and M.S. degree in aerospace engineering from Korea Advanced Institute of Science and Technology in 2013 and 2015, where he is currently working toward the Ph. D. course. His current research mainly focuses on UAV navigation technology.

Minchan Kim received the B.S. in aerospace engineering form Korea Aerospace University in 2011, and Ph.D. degree in aerospace engineering from Korea Advanced Institute of Science and Technology in 2017. His current research mainly focuses on GNSS augmentation systems and UAV navigation technology.

Jinsil Lee received the B.S. degree in civil and environmental engineering and Ph.D. degree in aerospace engineering from Korea Advanced Institute of Science and Technology in 2012 and 2019, respectively. Her current research interest is a multi-sensor navigation integrity system for unmanned vehicles.

Jiyun Lee received the B.S. degree in astronomy and atmospheric science from Yonsei University; the M.S. degree in aerospace engineering sciences from University of Colorado at Boulder; and the Ph.D. degree in aeronautics and astronautics from Stanford University in 2005. She is an Associate Professor with the Department of Aerospace Engineering, Korea Advanced Institute of Science and Technology. She has authored over 80 research papers in the field of GNSS applications, safety-critical systems.